A Cascaded Heading Control Design With Motion Constraint Handling for Marine Surface Vessels

Øivind K. Kjerstad[1] and Erlend M. Coates[2]

Abstract— Maritime motion control systems traditionally employ proportional-integral-derivative (PID) feedback control combined with a model-based feedforward structure for heading control. However, such control designs often suffer from the widely accepted limitation that the transient response from disturbances or significant measurement steps will not comply with operational motion constraints. This can pose a risk to onboard passengers and cargo, as the control law can impose motions that violate safety regulations. To address this limitation, we present a novel and simple control design that improves constraint handling while providing feasible rejection of external disturbances. Our design is based on a cascaded structure consisting of an outer-loop heading control law and an inner-loop rate-of-turn control law. The main contribution is the nonlinear feedback design of the outer-loop control law, which uses dynamic augmentation of the heading kinematics and nested saturation functions applied to the resulting second-order kinematics. We prove that the design is input-to-state stable with respect to the rate-of-turn error. The design has similar complexity as traditional designs with respect to implementation and tuning. The feasibility of the design is showcased with a simulation case study. The results demonstrate that the control design effectively handles operational constraints while maintaining good performance. The design has significant potential for real-world application in maritime motion control systems, as it provides a simple yet effective way to ensure compliance with operational constraints on heading rate and acceleration.

I. Introduction

Heading control is an essential component of maritime motion control systems that offers dynamic positioning (DP) or autopilot/trackpilot functionality. Its primary objective is to control the heading of a ship through its propulsion system so that its movement complies with a given system function. The motion control is typically subject to mechanical and operational constraints, such as maximum yawing moment and yawing moment rate from the propulsion system, as well as maximum yaw acceleration and rate-of-turn imposed by an operator for the safety and comfort of the cargo and passengers. In this paper, the focus and argumentation are centered around autopilot functionality, as it is standard equipment in almost all maritime vessels in commercial operation, but the results are relevant for any other maritime motion control function requiring heading control.

The autopilot control problem was tackled early in the twentieth century by pioneers such as Sperry, Minorski,

and others [1]. Their work, which was rooted in visual observation of how an experienced helmsman would steer a ship, led to the design of the proportional-integral-derivative (PID) control law [2]. Although various different formulations have emerged since then, including adaptive, linear quadratic, model-predictive, model-reference, H∞, L1 adaptive, sliding mode, and other approaches [3], [4], [5], [6], [7], [8], [9], variations of the PID design continue to be the most universally used for ship autopilot control systems [1]. For example, model-based PID-like approaches in [10] are considered by the authors to be state-of-the-art for real-world practical applications.

Typically, the literature on autopilot control designs consists of unconstrained heading control designs with an emphasis on theoretical aspects such as formulation derivation and stability properties. Little attention is paid to actuator, vessel, and operator constraints, although some publications include a maximum rudder angle, e.g., [11], [12]. One of the reasons for this is that the control design methodologies do not incorporate such constraints inherently, and they must be dealt with by ad-hoc methods, which often results in a loss of validity for the theoretical stability aspects. An alternative that can incorporate constraints is nonlinear model predictive control (NMPC). However, NMPC is not widely adopted for autopilot control designs, as it requires a precise model, which may be challenging to obtain, as well as requiring a numerical solver, making it more costly to implement and maintain relative to the methods mentioned above, especially in industrial legacy systems not centered around this control methodology. Nevertheless, some formulations exist, see, e.g., [13], [14], [15].

Today, operational motion constraints put on rate-of-turn and yaw acceleration are handled through the guidance system generating the control setpoint (see Figure 1). However, this typically only applies to planned maneuvers. Unplanned offsets resulting from measurement steps or significant disturbance perturbations will typically not comply with the motion constraints and will not be handled by the guidance system. Here, a measurement step refers to a sudden and significant change in the value of a signal, typically originating in a sensor or multi-sensor handling, but within the operational tolerances for allowing the sensor in the feedback loop. If the resulting setpoint offset is severe, it may result in transient motions that are unacceptable for passengers and cargo. Therefore, mitigating such scenarios through the control design serves as motivation for this paper. This challenge also borders on tuning, as autopilots often require gain scheduling to handle the entire velocity domain

[1]Øivind Kåre Kjerstad is with the Department of Ocean Operations and Civil Engineering, Faculty of Engineering, NTNU, Ålesund, Norway `oivind.k.kjerstad@ntnu.no`

[2]Erlend M. Coates is with the Department of ICT and Natural Sciences, Faculty of Information Technology and Electrical Engineering, NTNU, Ålesund, Norway `erlend.coates@ntnu.no`

with sufficient disturbance rejection and setpoint tracking performance. Tuning a maritime control system may be cumbersome and challenging if the weather, location, and time frame are sub-optimal. The potential outcome is that the autopilot has sub-optimal performance, resulting in higher fuel consumption and imprecise control performance. In turn, the autopilot may be frequently switched off, and manual steering used in operations where automatic control could be advantageous.

The main contribution of this study is a novel cascaded control design that enhances the transient performance of the control law. This is accomplished by utilizing a dynamic augmentation and a nested saturations control law [16] on the resulting second-order kinematics, which is rendered input-to-state stable w.r.t. the rate-of-turn error of the inner-loop. The outer-loop control law effectively serves as a dynamic acceleration and velocity-constrained reference filter to the inner-loop rate-of-turn control law. To describe and investigate this contribution, the paper is organized as follows: Section II outlines the scope and problem formulation, Section III presents the control design, Section IV features a simulation case study, and Section V discusses the results.

A. Notation and Definitions

For a function $f\colon \mathbb{R} \to \mathbb{R}$, $|f(t)|_a := \limsup_{t\to\infty}|f(t)|$ is the asymptotic bound of the function $f(t)$.

Our control strategy utilizes bounded controls and, in particular, *saturation functions* $\sigma\colon \mathbb{R} \to \mathbb{R}$ that satisfy [16]:

(P1) $|\sigma'(s)| := |d\sigma(s)/ds| \leq 2$, for all s,

(P2) $s\sigma(s) > 0$ for all $s \neq 0$, $\sigma(0) = 0$,

(P3) $\sigma(s) = \text{sgn}(s)$ for $|s| \geq 1$,

(P4) $|s| < |\sigma(s)| < 1$ for $|s| < 1$.

One way to generate such a function is to use polynomial interpolation, e.g. a cubic or quintic spline, where the degree of the polynomial can be chosen to achieve arbitrary smoothness of $\sigma(s)$.

II. SCOPE AND PROBLEM FORMULATION

Consider the following 3 degree-of-freedom (DOF) surface vessel model [10],

$$\dot{\eta} = R(\psi)\nu \tag{1a}$$
$$M\dot{\nu} + D(\nu)\nu + C(\nu)\nu = \tau + \tau_{wind} + \tau_{other} \tag{1b}$$

where $\eta = \begin{bmatrix} N_E & E_E & \psi \end{bmatrix}^\top$ is the north-east position and vessel heading, relative to some Earth fixed, north pointing coordinate systems, $R(\psi)$ is the rotation matrix between the Earth and body frames. $\nu = \begin{bmatrix} u & v & r \end{bmatrix}^\top$ is the vector of body-fixed velocities, M, $D(\nu)$, and $C(\nu)$ are the inertia matrix, the hydrodynamic damping matrix, and the Coriolis and centrifugal matrix, respectively. Further, τ_{wind} is the wind load, and τ_{other} is a collective term of all other influences from external sources such as currents and waves. Finally,

τ is the input control vector generated by the propulsion system. It can be defined as,

$$\tau = \begin{bmatrix} \tau_X & \tau_Y & \tau_N \end{bmatrix}^\top = f(v_r, n, \alpha), \tag{2}$$

where τ_X, τ_Y, and τ_N are the component forces in the different body-fixed DOFs. $f(\nu_r, n, \alpha)$ is a function relating the rpm of the propellers, n, the rudder or azimuth angle α, and the relative water velocity v_r to the force vector acting on the hull. This paper considers a conventional decoupled design where α is used to meet the heading control objective of tracking a time-varying reference signal $\psi_d(t)$ and n is kept under manual control.

By extracting the yaw-subsystem from (1), the yaw dynamics of the vessel can be written in the following general form [10]:

$$\dot{\psi} = r \tag{3}$$
$$(I_z - N_{\dot{r}})\dot{r} + N(u,v,r) = \tau_N + \tau_{wind,N} + \tau_{other,N} \tag{4}$$

where I_z is the moment of inertia, $N_{\dot{r}}$ is the added mass, and $N(u,v,r)$ is a function describing the hydrodynamic moment. The last two terms of (4) are the third components of τ_{wind} and τ_{other}, respectively. The level of fidelity of $N(u,v,r)$ is a key differentiator in the various autopilot designs. By selecting,

$$N(u,v,r) = N_r r, \tag{5}$$

where N_r is a hydrodynamic coefficient, a formulation highly similar to that of Nomoto, as seen in [17], is obtained. This is the most applied model for autopilot design in the literature by far. Another similar one is that of Norrbin [18]. Although these models have been successful, they are simplifying the physical phenomena extensively. To understand the magnitude and implications, consider the autopilot model developed in [19], where low aspect wing theory was applied using a Lagrange approach to derive a model with higher fidelity. This model can be stated as

$$\begin{aligned} N(u,v,r) =& N_{uv}^L uv + N_{uuv}^L u^2 v + N_{vvv}^L v^3 + N_{rrv}^L r^2 v \\ &+ N_{|v|v}|v|v + N_{|r|v}|r|v + N_{ur}^L ur + N_{uur}^L u^2 r \\ &+ N_{rrr}^L r^3 + N_{vvr}^L v^2 r + N_{|v|r}|v|r + N_{|r|r}|r|r \\ &- (X_{\dot{u}} - Y_{\dot{v}})uv + \frac{1}{2}(N_{\dot{v}} - Y_{\dot{r}})ru, \end{aligned} \tag{6}$$

where $X_{\dot{u}}, Y_{\dot{v}}, Y_{\dot{r}}$ and $N_{(\cdot)}$ are hydrodynamic coefficients. It is noteworthy that the cross-coupling terms with u and v, which may result in a significant dynamics change as a function of speed, are not present in (5). The alternative is to utilize (6) in the control design. However, this is also challenging due to the difficulty of obtaining accurate numerical values for all the coefficients. It is not considered in the scope of this paper to determine the most feasible feedforward structure for heading control, but the utilization of the model in the control structure will be partly addressed.

The objective of most heading control designs is to make ψ, r, $\dot{r}$ track some desired state ψ_d, r_d, $\dot{r}_d$, where, analogous

to (3),

$$\dot{\psi}_d = r_d. \tag{7}$$

The desired state is the output of a guidance module, as seen in Figure 1, which takes input from the autopilot operator. Typically, for motion control above about 4 knot, a decoupled design is considered so that τ_N is designed separately from τ_X, and τ_Y has no active control and is not considered explicitly. The reason why the ship needs some forward speed is the fact that for lower velocities the rudder effect of the propulsion is so low that it is difficult to use the main propulsion alone, as is typical for commercial autopilots, to generate sufficient yaw moment for effective control.

Since the model-based PID structure is considered state-of-the-art, it will be used as a benchmark comparison case here. The formulation is found in [10], and can be written as

$$\tau_N = \underbrace{(I_z - N_{\dot{r}})\dot{r}_d - \hat{\tau}_{wind} + \tau_{VFF}}_{\tau_{FF}}$$

$$+ \underbrace{K_p\tilde{\psi} + K_d(r_d - r) + K_i \int \tilde{\psi}dt}_{\tau_{FB}}, \tag{8}$$

where $\tilde{\psi} := \psi_d - \psi$ is the heading error, mapped to $[-\pi, \pi)$, τ_{FF} is the feedforward control terms, τ_{FB} is the feedback control terms, $\hat{\tau}_{wind}$ is an estimate of the wind loads, and K_p, K_i, and K_d are the proportional, integral and derivative control gains, respectively.

Most interesting in (8) is the design of τ_{VFF}. By using the Nomoto model of (5) this becomes,

$$\tau_{VFF} = N_r r_d. \tag{9}$$

Consider (8) designed with the Nomoto model feedforward, (9), inserted into (4) with the hydrodynamic definition in (6). This explains why such heading control designs behave poorly in dynamic scenarios with significant maneuvering and/or disturbance perturbations without gain scheduling or adaptation mechanisms. Simply put, the design does not capture the hydrodynamic effects, which get more influential with increasing velocity. Thus, it may be necessary to re-tune the heading control law at several operating points in order to handle the induced dynamics. Although resorting to a control design model that has higher fidelity may help, it does not solve the problem. For instance in a scenario when $\psi_d = $ constant and $\dot{r}_d = r_d = 0$, which is a major part of the autopilot operating profile, the feedback part of the controller must handle the perturbations, as $\tau_{VFF} = 0$. This shows that it may also be beneficial to design a control law that is able to utilize the hydrodynamic model during transient response instead of just in pre-planned situations.

It should be noted that this paper assumes that the heading and rate-of-turn measurements are available through an observer that filters out the first-order wave motion, when present. This is typically necessary in marine surface applications to avoid wear-and-tear on the propulsion system from high frequent wave modulation, as well as providing dead reckoning capabilities in the case of sensor signal loss.

III. CONTROL DESIGN

The heading control design is separated into two parts, as indicated by Figure 1. First, the outer-loop control law is presented. This is the main contribution of this work and it is responsible for the constrained control. It supplies a modified rate-of-turn and acceleration reference to the inner-loop control law that in turn utilizes the hydrodynamic model of the system during transient response. Our control strategy utilizes bounded controls and, in particular, saturation functions as defined in Section I-A.

A. Outer-Loop Heading Control

As shown in Figure 1, the desired reference trajectory is modified to accommodate the use of an inner-loop rate-of-turn control law. Thus, a mapping is proposed to ensure $\psi \to \psi_d$ while imposing motion constraints. This is defined as,

$$r_r = r_d + q \tag{10a}$$

$$\dot{r}_r = \dot{r}_d + \dot{q} \tag{10b}$$

where $q, \dot{q} \in \mathbb{R}$ are the modified trajectory components that ensure convergence to ψ_d. The objective of the inner-loop controller is then to control the rate-of-turn error $\tilde{r} := r_r - r$ to zero.

We want to impose constraints as follows:

$$|q| \le r_{max} \tag{11a}$$

$$|\dot{q}| \le a_{max}, \tag{11b}$$

where a_{max} is the maximum desired transient acceleration addition, and r_{max} the maximum desired transient rate-of-turn addition. To this end, we propose to assign the following dynamic, saturated feedback. First, let ξ be a virtual rate-of-turn reference ("the desired value for q") defined as

$$\xi = r_{\max}\sigma\left(\frac{k_\psi\tilde{\psi}}{r_{\max}}\right). \tag{12}$$

Now, to ensure that (11b) is fulfilled, let

$$\dot{q} = a_{\max}\sigma\left(\frac{k_q(\xi - q)}{a_{\max}}\right), \quad q(t_0) = q_0. \tag{13}$$

At this point, it should be noted that only (11b), and not (11a) is fulfilled. However, we do have $|\xi| \le r_{\max}$ by design. A practical solution is to saturate q as well. A sufficiently smooth saturation should be used since $\dot{r}_r$ appears in the expression for the inner-loop controller, (23). Solving this matter is the topic of future work.

The design parameters k_ψ, k_q are positive constants and should be chosen as described in the following proposition, which details the properties of the closed-loop system (inspired by [20]):

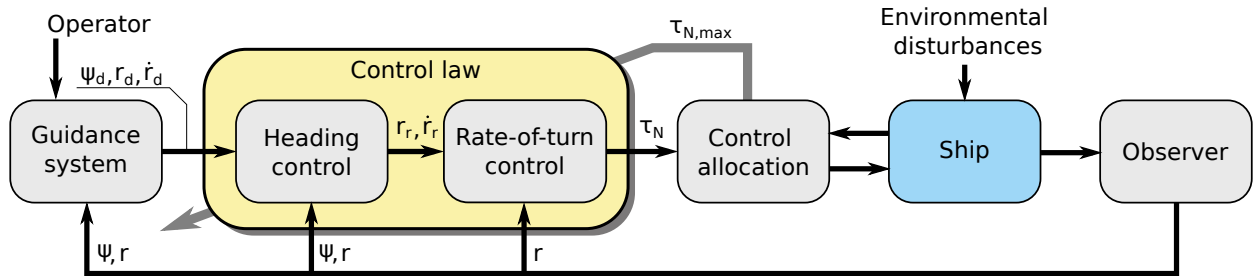*Proposition 1:* Consider the closed-loop system, consisting of (3), (7), (10a), and (12)-(13), with parameters

Fig. 1. Guidance, navigation and control structure of the proposed control law.

$k_\psi, k_q, a_{max}, r_{max}$ chosen such that

$$\frac{a_{max}}{k_q} < \frac{r_{max}}{4}, \quad 4k_\psi r_{max} < \frac{a_{max}}{4},$$
$$\frac{6k_\psi}{k_q} < \frac{1}{24}, \quad \tilde{r}_{max} < \frac{r_{max}}{4}, \tag{14}$$

for some $\tilde{r}_{max} > 0$. Then, the system is input-to-state stable (ISS) with respect to the input $\tilde{r}$, without restrictions on the initial state, with restriction $\tilde{r}_{max}$ on the input, and linear asymptotic gains. In particular, for all $\tilde{r}$ such that $|\tilde{r}|_\infty \leq \tilde{r}_{max}$, and for all initial conditions $(\tilde{\psi}(0), q(0)) \in \mathbb{R}^2$, the solutions are bounded and the heading error satisfies the asymptotic bound

$$|\tilde{\psi}|_a \leq \frac{2}{k_\psi^*}|\tilde{r}|_a. \tag{15}$$

Proof: Let $z_1 = \tilde{\psi}$ and $z_2 = \xi - q$. The system can be rewritten as

$$\dot{z}_1 = -r_{max}\sigma\left(\frac{k_\psi z_1}{r_{max}}\right) + z_2 + \tilde{r} \tag{16}$$

$$\dot{z}_2 = -a_{max}\sigma\left(\frac{k_q z_2}{a_{max}}\right) + k_\psi\sigma'\left(\frac{k_\psi z_1}{r_{max}}\right)\dot{z}_1. \tag{17}$$

The result follows from [16, Lemma C.2.1] since (16)-(17) is in the same form as [16, (C.7)] with $n = 2, q_1 = q_2 = 1, v_1 = \tilde{r}, v_2 = 0, \lambda_1 = r_{max}, \lambda_2 = a_{max}, K_1 = k_\psi$, and $K_2 = k_q$. ∎

Remark 1: It is well known that due to the topological properties of the unit circle (or equivalently, $SO(2)$), the heading angle ψ cannot be globally stabilized by continuous feedback [21]. The stated properties are based on the assumption that $\tilde{\psi} \in \mathbb{R}$ and not $S^1 := [-\pi, \pi)$. However, if $\tilde{\psi}$ is mapped to S^1 in the implementation of the controller, the result still holds.

Note that in the proof, $\tilde{r}$ is treated as an input (disturbance) variable. The responsibility of the inner-loop is to ensure that $|\tilde{r}|_\infty \leq \tilde{r}_{max}$. Then, in light of (15), if $\tilde{r}$ converges to zero, then so does $\tilde{\psi}$, from any initial state $\tilde{\psi}(t_0), q(t_0)$.

Finding $k_\psi, k_q, a_{max}, r_{max}$ that satisfy (14) can be challenging. However, a result in [16, Proposition C.2.2] lets us introduce a scaling factor $\epsilon > 0$ to transform a valid parameter set to another without re-checking all the conditions. Let $k_\psi^*, k_q^*, a_{max}^*$ and r_{max} satisfy (14). Now, the following set

of parameters k_ψ, k_q, a_{max} also satisfies (14) while at the same time respecting the constraint (11b):

$$k_\psi = \epsilon k_\psi^*, \quad k_q = \epsilon k_q^*, \tag{18}$$

with ϵ chosen as

$$0 < \epsilon \leq \frac{a_{max}}{a_{max}^*}. \tag{19}$$

The gain conditions given by (14) are also conservative. To increase the practical usefulness of the proposed control law, further insight is needed on the tuning of k_ψ and k_q for performance. One approach is to determine the characteristic polynomial of the closed-loop transfer function from $\tilde{\psi}(t_0)$ to $\tilde{\psi}$, which can be obtained by assuming that the errors are minor, i.e., $\tilde{r} \approx 0$ and $\tilde{\psi} \approx 0$, such that we can approximate the saturation function by its function arguments multiplied with its slope at zero, $\sigma'(0)$.

The characteristic polynomial can then be shown to be

$$c_O(s) = s^2 + \sigma'(0)k_q s + \sigma'(0)^2 k_\psi k_q \tag{20}$$
$$= s^2 + 2\zeta\omega_0 s + \omega_0^2, \tag{21}$$

where ω_0 is the natural frequency and ζ is the damping ratio. From this, a set of initial tuning rules can be developed as,

$$k_q = \frac{2\zeta\omega_0}{\sigma'(0)} \tag{22a}$$

$$k_\psi = \frac{\omega_0^2}{\sigma'(0)^2 k_q}. \tag{22b}$$

The initial tuning is then done by specifying desired values of ζ and ω_0 for the second-order characteristic polynomial. The value of $\sigma'(0)$ depends on the specific implementation of the saturation function. Practice has shown that this tuning approach yields good results and provides an understandable way of adjusting the system performance and response. Although (22) does not necessarily satisfy (14), the stability proof gives us confidence in the control architecture, and the additional tuning rules, (22) are helpful when faced with conservative conditions such as (14), which is inevitable in Lyapunov-based stability proofs.

B. Inner-Loop Rate-of-Turn Control

Due to the ISS property of the outer-loop heading controller, any stable and robust inner-loop control law for the rate-of-turn may be used along with the proposed outer-loop control

law. Thus, here the following control design, described in [22], is proposed,

$$\dot{\beta} = \dot{r}_r + k_i \tilde{r} \tag{23a}$$

$$\tau_N = (I_z - N_{\dot{r}})\dot{r}_r + \tau_{VFF} + k_p(\beta - r), \tag{23b}$$

where k_p and k_i are positive control gains. This is essentially a PI controller with model feedforward, and any formulation with similar characteristics may be used. τ_{VFF} is defined as,

$$\tau_{VFF} = N(u_d, v_d, r_r), \tag{24}$$

where u_d and v_d are setpoints for surge and sway velocities. It should be noted that u_d will only be available when the surge velocity is under automatic control and not during thrust-, power-, or manual control modes. In that case, $u_d = u$ may be used. Similarly, v_d is typically not available. Thus, $v_d = v$ or $v_d = 0$ may be used.

Analyzing the stability of the proposed rate-of-turn control law in the unconstrained case is trivial if the Nomoto model in (5) and (9) is used. However, this is of little point as the Nomoto model is insufficient in a dynamic scenario. Secondly, the control law will occasionally encounter hard saturation limits in the propulsion system. Nevertheless, due to the ISS property of the outer loop, imperfections in the inner-loop control will not deteriorate the overall performance of the cascaded control loop.

Tuning of the proposed inner-loop control law can be done by determining the characteristic equation of the first-order transfer function and ensuring that its bandwidth is sufficiently higher than the outer loop. This completes the total cascaded control design covering the most important aspects.

C. Complementary Issues

To avoid integral wind-up challenges when the control signal exceeds the capability of the propulsion system, conditional integration can be applied as,

$$\dot{q} = \begin{cases} 0 & \text{if } |\tau_N| > \tau_{N,max} \text{ and} \\ & \quad \tau_N(r_r - r) > 0 \\ a_{\max}\sigma\left(\frac{k_q(\xi - q)}{a_{\max}}\right) & \text{otherwise,} \end{cases} \tag{25}$$

where $q(0) = r - r_d$. This detects when integrator overflow will occur and sets the rate to zero by using a simple switch.

IV. SIMULATION STUDY

The simulation study compares the proposed control design with that of PID using a model of the RV Gunnerus. Traditionally, it isn't easy to evaluate the performance objectively as it comes down to the specific tuning. However, in this case, matching the natural frequency of a second-order closed-loop PID approximation with that of the proposed outer-loop control law tuned according to (22b) will give some insight, albeit we acknowledge that the validity is best when $\tilde{r} \approx 0$. The applied tuning rules for the model-based PID heading control law can be found in [10] as $K_p = (I_z - N_{\dot{r}})\omega_0^2$, $K_d = 2\zeta\omega_0(I_z - N_{\dot{r}})$, and $K_i = \frac{\omega_0 K_p}{10}$.

The model (1) was set to represent RV Gunnerus where the mass, added mass and hydrodynamic coefficients were identified using a mix of ShipX [23] and a least-squares fit to a dataset of maneuvering trials. The propulsion system, which can be seen in Figure 2, was modeled in two parts: first, the steering gear dynamics were modeled as a second-order rate-limited process, and second, the thrust and rudder effects were implemented by using the manufacturer thrust curves complemented with added lift and drag effects induced by the nozzle. More specifically, we model $f(v_r, n, \alpha)$ in (2) as

$$f(v_r, n, \alpha) = \sum_{i=1}^{2} \begin{bmatrix} F_{x,i} & F_{y,i} & l_{x,i}F_{y,i} - l_{y,i}F_{x,i} \end{bmatrix}^\top, \tag{26}$$

where $l_{x,i}$ and $l_{y,i}$ for $i \in \{1, 2\}$ are the planar body frame distances in surge and sway, respectively, from the vessel CO to the thrusters' mounting positions. The individual thrusters are modeled as,

$$F_{x,i} = T_i \cos(\alpha) - D_i(\alpha, u, v, r) \tag{27a}$$

$$F_{y,i} = T_i \sin(\alpha_i) + L_i(\alpha, u, v, r) \tag{27b}$$

$$T_i = K_T(n, \alpha, u, v, r)\rho D_p^4 |n|n \tag{27c}$$

$$D_i(\alpha, u, v, r) = 0.5 C_D(\alpha_i)\rho A V_{a,i}(u, v, r)^2 \tag{27d}$$

$$L_i(\alpha, u, v, r) = 0.5 C_L(\alpha_i)\rho A V_{a,i}(u, v, r)^2 \tag{27e}$$

where $F_{x,i}$ and $F_{y,i}$ are the local body-aligned forces at the location of the thruster, D_i and L_i are the induced drag and lift forces, K_T is a thrust coefficient function approximated from thruster vendor data, ρ is the density of water, D_p is the propeller diameter of 1.9 meters, C_L and C_D are the lift and drag coefficients, respectively, A is the nozzle rudder area, and $V_{a,i}$ is the approximated water inflow velocity to the thruster under the assumption of zero current. Since C_L and C_D were unavailable, C_L was modeled linearly within the stall angle with a relatively low maximum value at 0.4 to account for the fact that it is not an actual rudder, but a nozzle that has some rudder effect. Further, the stall angle of the nozzle rudder effect was also set relatively low, at 25 degrees. In the simulation provided here, the operational angle available to the control system was set not to exceed this limit. C_D was modeled quadratically with $C_D(0) = 0.01$ and $C_D(90°) = 1.2$. It should be noted that the tunnel thruster of RV Gunnerus was not modeled here as it is not used during autopilot operations. To simplify the simulation, wind and wave loads were not explicitly implemented, but a cumulative time-varying signal was used to approximate external disturbances. We utilized a numerical search-based control allocation method to determine a single azimuth angle α from τ_N, resulting in an equal rudder angle for all actuators, similar to commercial autopilots.

This study considered a scenario where the vessel is exposed to acceleration, deceleration, maneuvering, and external disturbances. The vessel heading was initialized 45 deg off the setpoint to show the transient behavior of the closed-loop systems subject to significant setpoint deviation. After 300 seconds, a kinematic constant jerk guidance model, similar to that of [24], is used to generate a trajectory for changing the

Fig. 2. RV Gunnerus in dock showing the two stern rim-driven azimuth thrusters. Courtesy of Kongsberg Maritime AS

heading setpoint from the initial 10 degrees to 140 degrees. It must be mentioned that this is an open-loop approach that computes a trajectory from the previous setpoint to the next disregarding the vessel state. Similar methods are also seen in [10]. After 350 seconds, a disturbance is introduced to display the disturbance rejection capabilities of the control laws (see Figure 3). Both control laws were set up with $\omega_0 = 0.1$ and $\zeta = 1.1$. For the proposed control law, r_{max} were set to 60 deg/min and a_{max} to 3 deg/s². We used a quintic spline to implement a saturation function, where $\sigma'(0) = 1.2$. The resulting gain values, $k_q = 0.183$ and $k_\psi = 0.038$ according to (22), do not satisfy all of the (conservative) conditions in (14) but has led to good results in simulations. A feedforward model based on (6) was applied for both control laws. However, in the case of the proposed control law, r_d was replaced with r_r as seen in (24). The control gains k_i and k_p of (23) were set to 0.0455 and 9.12×10^6, respectively. Both control laws were implemented with conditional integration to limit integral windup when subject to the mechanical or operator-set maximum azimuth angle. The simulation was performed with a variable step length of maximum 0.01 seconds.

Figure 3 displays the simulation results, highlighting the favorable properties of the proposed control law compared to the traditional PID control law. During the first phase of the simulation (0 to 100 seconds), where the vessel converges to the setpoint from an initial offset without a guiding trajectory ($\dot{r}d = r_d = 0$), the proposed control law demonstrates superior performance. It achieves this by not overshooting and limiting the rate-of-turn according to the predefined $rmax$ and a_{max}, as evidenced by the behavior of $\dot{q}$ and q. In contrast, the PID control law, which lacks constraint-limiting mechanisms, does not produce such behaviour. During the second phase of the simulation (100 to 550 seconds), where the vessel follows a predefined trajectory, both control laws perform similarly due to the driving nature of the constant jerk guidance scheme and the equal tuning employed in both designs. In the third phase (550 to 1000 seconds), where the vessel encounters a time-varying disturbance, the proposed control law demonstrates improved disturbance rejection with minimal impact on the allocated azimuth angle

compared to the PID. The proposed control law accomplishes this by utilizing the rate-of-turn deviation more heavily in disturbance rejection, as opposed to heading deviation, which is the case for the PID. As a result, the proposed control law improves the phase properties of the rejection mechanism and can respond to disturbances earlier, leading to better overall performance. This can also be verified by the normalized performance indexes in the figure, defined as $KPI_\psi = \int_0^t |\tilde{\psi}| dt$ and $KPI_{\ddot{\alpha}} = \int_0^t |\ddot{\alpha}| dt$. Especially, $KPI_{\ddot{\alpha}}$ indicate that the azimuth angle accelerations, and thereby the wear-and-tear on the steering mechanisms, is not increased to accommodate for the increase in performance seen in KPI_ψ.

V. DISCUSSION

The proposed control law presents significant advantages over traditional and popular model-based PID control laws for heading control of maritime surface vessels. First, it incorporates constraint handling while also improving disturbance rejection. Second, it enables the use of the model-based feedforward structure in situations where $\tilde{\psi} \neq 0$ and $\dot{r}_d = r_d = 0$, which is the most common operational scenario for autopilots. In such cases, the model-based PID control law would rely solely on feedback setpoint error terms, which can lead to poor performance due to unhandled velocity-dependent hydrodynamic effects. However, the proposed control law overcomes this limitation by allowing the feedforward structure to compensate for these effects. It is important to note that this advantage is dependent on the accuracy of the hydrodynamic model used in the control law. If the model is inaccurate, the benefit of the proposed control law may be reduced.

The proposed control law also includes relatively simple tuning laws, which make it simple and intuitive to implement. Moreover, it does not add additional tuning or implementation complexity compared to model-based PID control laws. As such, it may be an attractive alternative for practitioners who seek to improve disturbance rejection and constraint handling without incurring additional complexity. It is worth noting that, to the best of the authors' knowledge, there is currently no deterministic control design available that offers the presented capabilities for maritime heading control of surface vessels. This makes the paper a promising contribution to be pursued further and evaluated in full-scale experiments.

REFERENCES

[1] G.N. Roberts, R. Sutton, A. Zirilli, and A. Tiano. Intelligent ship autopilots—a historical perspective. *Mechatronics*, 13(10):1091–1103, 2003. Mechatronics - a 12 year celebration.

[2] S. Bennett. Nicholas minorsky and the automatic steering of ships. *IEEE Control Systems Magazine*, 4(4):10–15, 1984.

[3] Jasmin Velagic, Zoran Vukic, and Edin Omerdic. Adaptive fuzzy ship autopilot for track-keeping. *Control Engineering Practice*, 11(4):433–443, 2003. MCMC00.

[4] Haitong Xu, P. Oliveira, and C. Guedes Soares. L1 adaptive backstepping control for path-following of underactuated marine surface ships. *European Journal of Control*, 58:357–372, 2021.
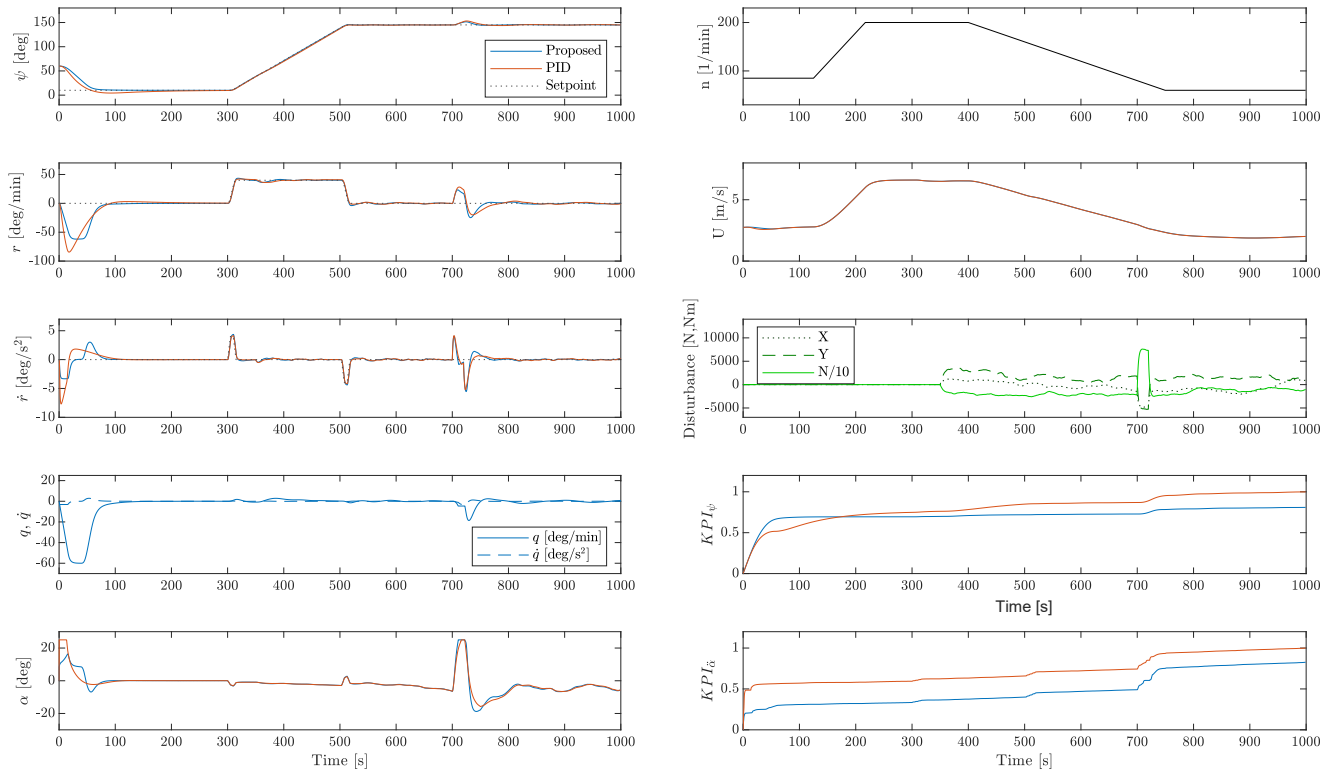
Fig. 3. The results of the simulation case study including acceleration, deceleration, maneuvering, and disturbance-rejection phases. Note that the vessel speed is defined as $U = \sqrt{u^2 + v^2}$.

[5] Zhen Li and Jing Sun. Disturbance compensating model predictive control with application to ship heading control. *IEEE Transactions on Control Systems Technology*, 20(1):257–265, 2012.

[6] C.G. Källström, K.J. Åström, N.E. Thorell, J. Eriksson, and L. Sten. Adaptive autopilots for tankers. *Automatica*, 15(3):241–254, 1979.

[7] Mirosław Tomera. Nonlinear controller design of a ship autopilot. *International Journal of Applied Mathematics and Computer Science*, 20(2):271–280, 2010.

[8] J. Van Amerongen and A.J. Udink Ten Cate. Model reference adaptive autopilots for ships. *Automatica*, 11(5):441–449, 1975.

[9] Thor Fossen. High performance ship autopilot with wave filter. *Proceedings of the 10th International Ship Control Systems Symposium*, 03 1995.

[10] Thor I Fossen. *Handbook of marine craft hydrodynamics and motion control*. Wiley, June 2021.

[11] Jialu Du, Xin Hu, and Yuqing Sun. Adaptive robust nonlinear control design for course tracking of ships subject to external disturbances and input saturation. *IEEE Transactions on Systems, Man, and Cybernetics: Systems*, 50(1):193–202, 2020.

[12] Ching-Yaw Tzeng and Kang-Fu Lin. Adaptive ship steering autopilot design with saturating and slew rate limiting actuator*. *International Journal of Adaptive Control and Signal Processing*, 14(4):411–426, 2000.

[13] Wenxin Wang and Cheng Liu. An efficient ship autopilot design using observer-based model predictive control. *Proceedings of the Institution of Mechanical Engineers, Part M: Journal of Engineering for the Maritime Environment*, 235(1):203–212, 2021.

[14] Andy S. K. Annamalai and Amit Motwani. A comparison between lqg and mpc autopilots for inclusion in a navigation, guidance and control system. 2013.

[15] Tahiyatul Asfihani, Khusnul Chotimah, Irma Fitria, and Subchan. Ship heading control using nonlinear model predictive control. In *2020 3rd International Seminar on Research of Information Technology and Intelligent Systems (ISRITI)*, pages 306–309, 2020.

[16] Alberto Isidori, Lorenzo Marconi, and Andrea Serrani. *Robust Autonomous Guidance*. Springer London, 2003.

[17] K. Nomoto, T. Taguchi, K. Honda, and S. Hirano. Steering qualities of ships. *International Shipbuilding Progress*, 4(35):354–370, 1957.

[18] N. H. Norrbin. On the design and analyses of the zig-zag test on base of quasi linear frequency response. Technical report, The Swedish State Shipbuilding Experimental Tank (SSPA), 1963.

[19] Andrew Ross. *Nonlinear Manoeuvring Models for Ships: a Lagrangian Approach*. PhD thesis, Norwegian University of Science and Technology, 2008.

[20] Roberto Naldi, Michele Furci, Ricardo G. Sanfelice, and Lorenzo Marconi. Robust global trajectory tracking for underactuated VTOL aerial vehicles using inner-outer loop control paradigms. *IEEE Transactions on Automatic Control*, 62(1):97–112, jan 2017.

[21] Sanjay P. Bhat and Dennis S. Bernstein. A topological obstruction to continuous global stabilization of rotational motion and the unwinding phenomenon. *Systems & Control Letters*, 39(1):63–70, jan 2000.

[22] Øivind K. Kjerstad, Svenn Are T. Værnø, and Roger Skjetne. A robust dynamic positioning tracking control law mitigating integral windup. *IFAC-PapersOnLine*, 49(23):239–244, 2016. 10th IFAC Conference on Control Applications in Marine Systems CAMS 2016.

[23] Marintek. Shipx fact sheet. Printed brochure.

[24] Daniel A. Fernandes. *An output feedback motion control system for ROVs*. PhD thesis, Norwegian University of Science and Technology, 2015.